

# Laser-Driven Magnetic-Flux Compression in High-Energy-Density Plasmas

In the magnetic-fusion-energy (MFE) concept, a strong magnetic field confines the plasma and reduces the electron thermal conduction to the vessel wall.<sup>1</sup> The magnetic pressure of typical  $\sim 0.1$ -MG fields in MFE is higher than the total energy density of the plasma (with  $\beta = 2\mu_0 p/B^2 < 1$ ). MFE plasmas are fully magnetized and characterized by a Hall parameter  $\omega_{ce}\tau \gg 1$  since the modest gyrofrequency  $\omega_{ce}$  is matched by long collision times  $\tau$ . In contrast, typical inertial confinement fusion (ICF) plasmas have collision frequencies higher by 10 to 12 orders of magnitude because of their extreme density. In such systems, thermal conduction losses are a major factor in the energy balance of an implosion. While it may be more difficult, magnetizing the hot spot in ICF implosions can lead to improved gain in implosions of massive targets with relatively low implosion velocity<sup>2</sup> or to a reduction of the energy required for ignition. However, tens of MG are needed to achieve  $\omega_{ce}\tau \sim 1$  in the hot spot of a typical direct-drive DT ignition target<sup>3</sup> with a hot-spot density of  $\sim 30$  g/cc and a temperature of  $\sim 7$  keV. Such a field is higher than both the self-generated magnetic fields (see Ref. 4) and the external fields that can be generated by coils. Magnetic-flux compression<sup>5</sup> is a viable path to generating tens-of-MG magnetic fields with adequate size.<sup>6</sup> Magnetic-flux compression has been successfully achieved using the radial compression of a metallic liner driven by high explosives<sup>7,8</sup> or by pulsed power. The latter approach has been pursued by the Z-pinch<sup>9</sup> (including wire-array targets) and magnetized-target-fusion<sup>10</sup> communities. The results from the first experiments on a new approach that provides very effective flux compression are reported here. The field is compressed by the ablative pressure exerted on an imploding ICF capsule by the driving laser.<sup>11</sup> This approach was proposed in the 1980s (Ref. 12) as a way to achieve record compressed fields with possible applications for fusion,<sup>13</sup> but no laser experiments were performed. There are numerous advantages to this approach because the implosion velocity is high (a few  $10^7$  cm/s) and the hot plasma is an effective conductor that traps the embedded (seeded) initial magnetic field with minimal resistive diffusion. This approach can be used to magnetize high-energy-density plasmas for a number of applications ranging from controlled fusion to laboratory astrophysics.

Figure 119.5 describes a cylindrical implosion on OMEGA that used axial seed fields embedded in the target prior to compression.<sup>14</sup> The target was a  $20\text{-}\mu\text{m}$ -thick, 0.86-mm-diam CH cylindrical shell filled with D<sub>2</sub> gas. Some of the physical details of this concept are described in Refs. 11 and 15. The shock-heated and ionized D<sub>2</sub> fuel traps the seed magnetic field, which would otherwise diffuse much faster through the relatively cold (resistive) imploding shell. The seed field was provided by a Helmholtz-like double coil [Fig. 119.6(a); coil diameter and separation are both 4 mm], coaxial with the cylindrical target.<sup>16</sup> The more-complicated min-B magnetic geometries used in magnetic-confinement-fusion (MCF) magnetic mirror experiments were not used here because the magnetohydrodynamic (MHD) instability must be considered more carefully. A portable capacitive discharge system<sup>16</sup> delivers up to 80-kA current to the coils. The on-axis seed field was 50 to 90 kG at the target and 120 to 160 kG in the coil planes because of the coil separation chosen to avoid obscuring laser beams.

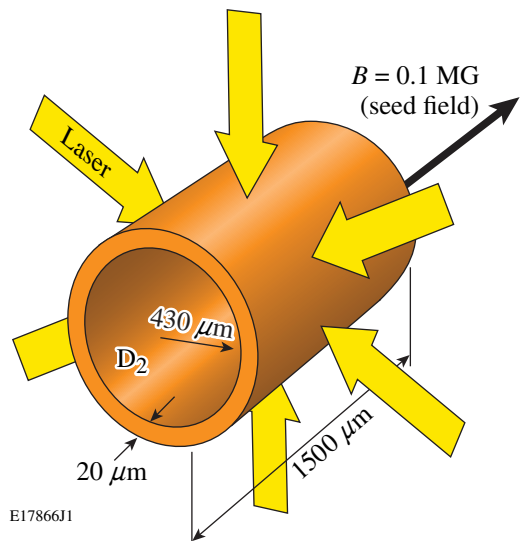


Figure 119.5  
Laser-driven flux compression in a cylindrical target. A D<sub>2</sub>-gas fill inside the plastic shell traps the seed field after shock ionization.

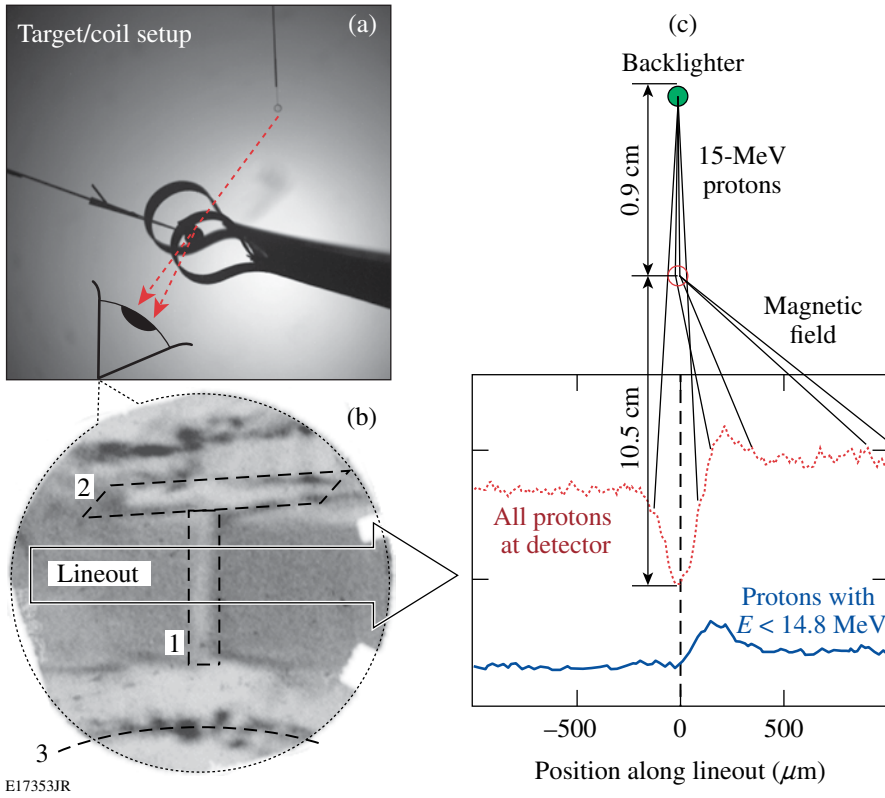


Figure 119.6

(a) Photo of the target/coil setup. (b) Proton density map for shot 51069. Darker areas represent higher fluence: (1) compressed core, (2) target plug, and (3) coil shadow. (c) Lineouts in two energy bands expose the deflected protons ( $E_k < 14.8$  MeV, solid line; all protons, dotted line).

The compressed fields within the dense, optically thick ICF plasmas are difficult to measure. Proton deflectometry based on the method described in Refs. 17–19 is a viable diagnostic that has been implemented on OMEGA. A monoenergetic ( $\Delta E/E \sim 0.03$ ), point-like (size/object distance  $\sim 0.01$ ), time-gated (an  $\sim 150$ -ps burst) proton source is provided by a glass sphere, filled with D<sup>3</sup>He gas and driven in an exploding pusher scheme by several tightly focused OMEGA beams. The 14.7-MeV protons produced by the D-<sup>3</sup>He fusion reactions are accelerated to  $\sim 15.2$  MeV by charging the backlighter target and recorded on a CR-39 nuclear track detector that provides both spatial and energy resolution (via the track diameter) of the particles incident on the surface.<sup>20</sup> The data [Fig. 119.6(b)] were generated as a convolution in space (source size, scattering at the object and detector) and time (finite duration) of the proton burst interacting with the field and target structure. None of the radial striations reported in Ref. 18 for spherical implosions was seen around the compressed core in these experiments, possibly because the target was imaged more than a nanosecond after the laser was

turned off. Turbulent field structure was present around the target plugs and stalk, but, while interesting, its morphology is beyond the scope of this article and will not be discussed.

A discrimination of tracks by energy (track diameter) was implemented to separate the core- (strong-field) traversing protons from the background, “free-space” particles that land in the same area of the detector. This is shown in Fig. 119.6(c), where the proton density map for shot 51069 [Fig. 119.6(b)] was used to construct two lineouts by taking a band of data and averaging over its width. The lower curve in Fig. 119.6(c) is from tracks with only energy  $E_k < 14.8$  MeV caused by an additional slowdown through the magnetized target. It shows an asymmetric peak in the proton density caused by deflection in the target field. In contrast, the data from multiple “null” experiments performed to establish the particle-density pattern for implosions with no seed field retain central symmetry in the cross-core lineouts (Fig. 119.7); i.e., the low-energy peak lines up with the trough of the high-energy proton lineout.

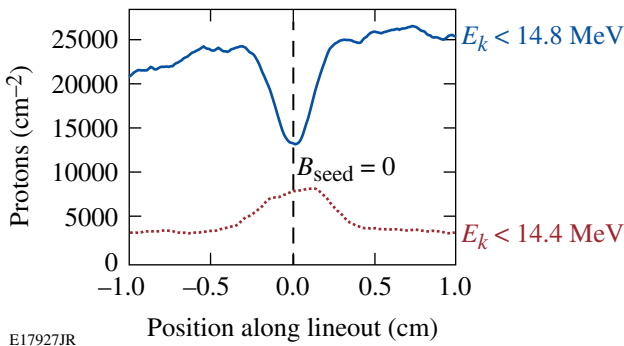


Figure 119.7

Cross-core lineouts from proton radiograph of shot 49693—an implosion with no external magnetic field—show that the core-traversing protons remained undeflected.

To predict and interpret the experimental data, a simulation package based on the Monte Carlo (MC) particle-transport framework Geant4 (Ref. 21) was developed. After including the field topology and material parameters predicted by the *LILAC-MHD* code<sup>22</sup> for the time of proton probing, the particle-transport code computes the deflection pattern under the combined action of the field and scattering/energy-loss processes. A comparison (Fig. 119.8) of the MC simulation predictions (solid) and experimental data (dotted) for shot 49704, in which a compressed field of 13 MG was predicted by the hydrocode, shows very good agreement in both the total fluence and low-energy-band lineouts. In Fig. 119.8(b), only the protons that had an incident energy lower than 14.8 MeV were included. The target in shot 49704 had a seed field of 10 kG and was probed relatively early in the implosion. In later experiments, where the proton burst occurred at or near peak compression, the experimental lineouts at intermediate energies exhibited a double-deflection pattern with a second deflection peak farther from the center [Fig. 119.9(a), shot 51069]. This was first seen in Monte Carlo simulations [Fig. 119.9(b)] and was caused by an abrupt jump of the field in the small volume of the hot spot from much lower values in the shell (responsible for the first deflection). Early in time, at a low compressed field, these two peaks were essentially merged, as is the case with shot 49704. A comparison of the data for shot 51069, which had a 56-kG seed field, and the simulation shows good qualitative agreement, capturing the double-peak-deflection pattern. The protons that were slowed down the most (dashed-dotted curve) were those that crossed through the shell but not the hot spot, missing the peak field. From the 1.9-cm deflection of the secondary peak, one can estimate an average product  $\langle R_B B_{\max} \rangle \approx 2\theta e/m_p v_p$  of 0.052 Tm, corresponding to an ~30-MG hot-spot field for a predicted hot-spot size of 17  $\mu\text{m}$ .

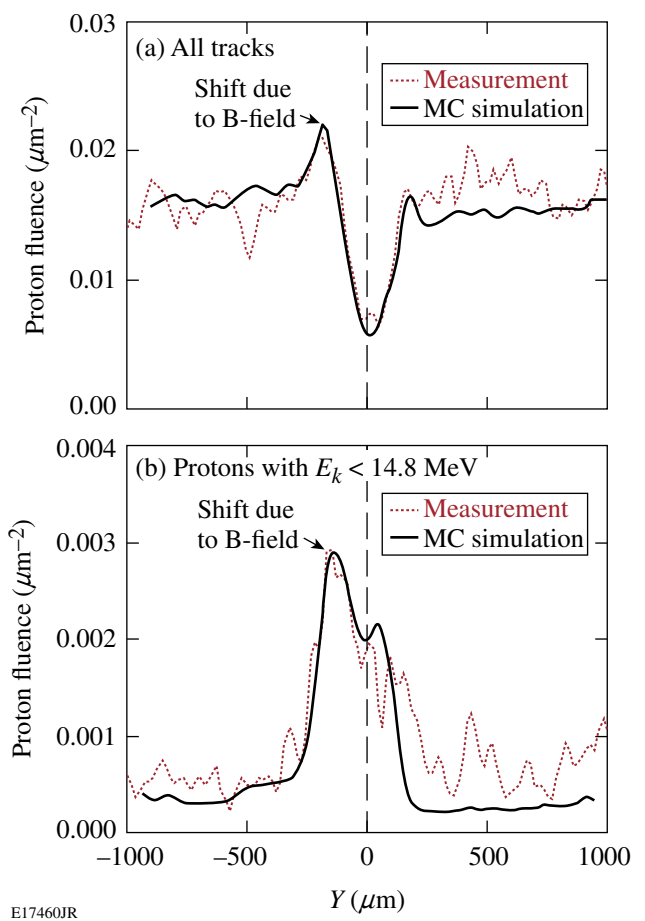


Figure 119.8

Direct comparisons of measured (dotted) and MC simulated (solid) proton-density lineouts across the core in shot 49704: (a) all protons; (b) protons intercepting the target ( $E_k < 14.8$  MeV) (isolated by track diameter).

When the seed-field direction was reversed (by reversing the current in the coils), the deflection pattern (Fig. 119.10, shot 52532) reversed direction, with the deflection now away from the target stalk (a spatial reference fixed for all shots). This confirms the magnetic nature of the deflection and supports the “relocation” of the high-field deflection to the other side of the core. This is also evident in lineouts at several energies shown in Fig. 119.10(b), where, in addition to the offset peak near the center (at ~2.5 cm), there is again a concentration of tracks away from it (at 0.4 cm), caused by the peak of the compressed field in the hot spot. Analysis of the second peak deflection in shot 52532 revealed that the higher seed field (~62 kG), as compared to shot 51069, was amplified to at least ~36 MG. The larger second peak area for Fig. 119.10(b) suggests higher hot-spot uniformity as more protons fall into these energy bands after being slowed down. The fields determined from Figs. 119.9 and 119.10 are the most conservative values, given

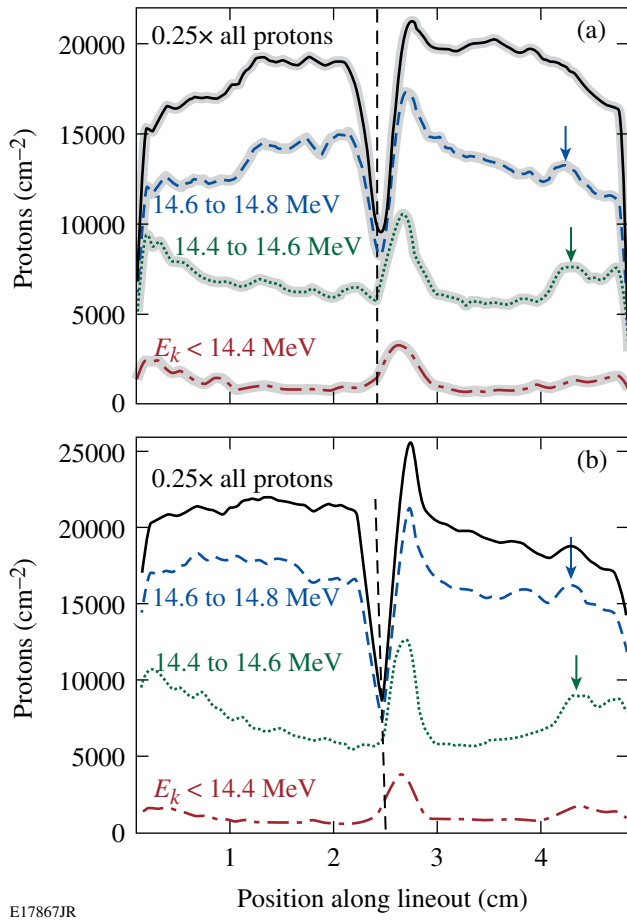


Figure 119.9

(a) Partitioning of the data in energy bands for shot 51069 exposed the protons that traverse the high field in the target center. (b) Partitioning in energy bands in the Monte Carlo simulation. The arrows in these plots indicate a second deflection peak at 1.9 cm from the target center.

by the lowest field  $B_{\max}$ , spread over the largest radius  $R_B$ , that can result in the observed deflection  $\theta \sim \langle R_B B_{\max} \rangle$  without violating the flux conservation condition  $\Phi \sim \langle R_B^2 B_{\max} \rangle \leq \Phi_0$ . If the more realistic case is considered, where up to 40% of the initial magnetic flux ( $\Phi_0 \approx 360 \text{ G cm}^2$ ) is lost as predicted by the hydro simulation, the estimated magnetic fields must be revised upward to match the observed deflections.

The effect of the amplified magnetic field on the hot-spot conditions was expected to be rather small for this experimental configuration. The 1-D hydrocode predicts a 2 $\times$  to 3 $\times$  increase in the yield caused by the temperature increase from thermal insulation in the hot spot. Note that higher temperatures are accompanied by lower hot-spot densities (Fig. 119.11, solid line) and lower plasma pressures since the total pressure (plasma + magnetic) is approximately independent of the magnetic field

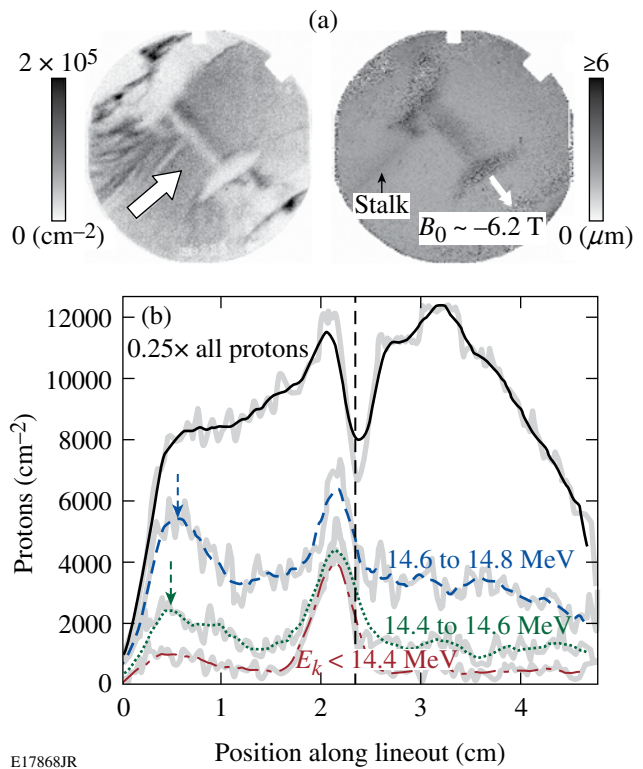


Figure 119.10

(a) Proton track density and diameter maps for shot 52532. The stalk is on the left, and deflection is to the right (seed field reversed). (b) Smoothed total (solid) and reduced-energy-band lineouts show large deflection matching a compressed field  $>36 \text{ MG}$ . The arrows in (b) indicate the second deflection peak.

(the minimum volume-averaged hot-spot beta is  $\sim 300$ , but is of the order of unity in the center). The highest neutron yield of  $5.8 \times 10^8$  was measured in shot 49704 with a 10-kG seed field. With the present setup, however, and due to target parameter variations (gas pressure, orientation, positioning, and build quality), the  $B_0 = 0$  yields already have variations of more than a factor of 3 (between  $7.7 \times 10^7$  and  $4.5 \times 10^8$ ). Such large shot-to-shot variations prevent an accurate assessment of the fusion yield enhancement caused by magnetic insulation. In addition, the scale of the experiment is such that the hot-spot ions most likely to undergo fusion reactions (at the Gamow peak) are essentially in the kinetic regime. This can be seen from Table 119.I, where  $n_{e,\text{hs}} = 8 \times 10^{22} \text{ cm}^{-3}$ ,  $T_{\text{hs}} = 1.5 \text{ keV}$ , the Gamow peak is at 8.2 keV, and the Coulomb logarithms for the collisions of the 8-keV ions with thermal electrons and ions are  $\Lambda_{ie} \approx 5$  and  $\Lambda_{ii} \approx 8.6$ , respectively. It is clear that the ions, having an  $\sim 6\text{-}\mu\text{m}$  mean free path, will undergo only a few collisions before leaving the hot spot. The electrons are fully magnetized but are thermally decoupled from the ions since the thermal equilibration time is of the order of 100 ps.

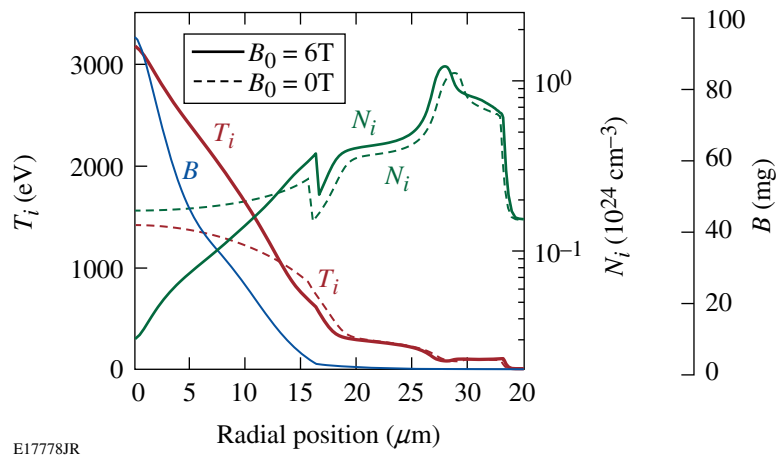


Figure 119.11

Ion temperature ( $T_i$ ) and density ( $N_i$ ) from *LILAC-MHD* simulations with (solid line) and without (dashed line) the magnetic field show that, along with a temperature increase caused by the magnetic field, a drop in the hot-spot density is predicted.

Table 119.I: Collision frequency ( $\nu_{ie}$ ,  $\nu_{ii}$ ), Hall parameter of ions ( $\omega_{ci}/\nu_{ii}$ ), mean free paths, and Larmor radii for a simulated cylindrical magnetized hot spot ( $R = 18$  mm) with an averaged field of 30 MG.

$\nu_{ie}$ ns <sup>-1</sup>	$\nu_{ii}$ ns <sup>-1</sup>	$\omega_{ci}/\nu_{ii}$	mfp <sub>ie</sub> μm	mfp <sub>ii</sub> μm	$r_L$ , μm
5.4	147	0.97	151	5.6	5.7

The situation should improve significantly in planned spherical magnetized implosions where the hot-spot density and collisionality are significantly higher.

In summary, very high magnetic-flux compression has been achieved using the ablative pressure of the OMEGA laser to drive a cylindrical shell at high implosion velocity, trapping and compressing the embedded external field to tens of MG, high enough to magnetize the hot-spot plasma. Finding the parameter space where target performance will be most affected by the compressed magnetic field is the next step in these studies.

#### ACKNOWLEDGMENT

The authors thank Dr. F. Y. Thio and Dr. A. Velikovich for many illuminating discussions and for their encouragement in pursuing these novel experiments. This work was supported by the U.S. Department of Energy Office of Fusion Energy Sciences under Grants DE-FG02-04ER54768 and DE-FC02-ER54789 and by the Office of Inertial Confinement Fusion under Cooperative Agreement No. DE-FC52-08NA28302, the University of Rochester, and the New York State Energy Research and Development Authority. The support of DOE does not constitute an endorsement by DOE of the views expressed in this article.

#### REFERENCES

- J. A. Wesson, *Tokamaks*, 3rd ed. (Clarendon Press, Oxford, 2004); A. H. Boozer, Rev. Mod. Phys. **76**, 1071 (2004).
- R. Betti, K. Anderson, T. R. Boehly, T. J. B. Collins, R. S. Craxton, J. A. Delettrez, D. H. Edgell, R. Epstein, V. Yu. Glebov, V. N. Goncharov, D. R. Harding, R. L. Keck, J. H. Kelly, J. P. Knauer, S. J. Loucks, J. A. Marozas, F. J. Marshall, A. V. Maximov, D. N. Maywar, R. L. McCrory, P. W. McKenty, D. D. Meyerhofer, J. Myatt, P. B. Radha, S. P. Regan, C. Ren, T. C. Sangster, W. Seka, S. Skupsky, A. A. Solodov, V. A. Smalyuk, J. M. Soures, C. Stoeckl, W. Theobald, B. Yaakobi, C. Zhou, J. D. Zuegel, J. A. Frenje, C. K. Li, R. D. Petrasso, and F. H. Séguin, Plasma Phys. Control. Fusion **48**, B153 (2006).
- P. W. McKenty, V. N. Goncharov, R. P. J. Town, S. Skupsky, R. Betti, and R. L. McCrory, Phys. Plasmas **8**, 2315 (2001).
- J. A. Stamper, Laser Part. Beams **9**, 841 (1991).
- Fields of 10<sup>8</sup> G have been associated with the high-current electron beams created in short-pulse laser-plasma interactions, but the small scale of these azimuthal fields precludes their use for hot-spot thermal insulation in ICF.
- F. Herlach, Rep. Prog. Phys. **31**, 341 (1968); F. Herlach, Rep. Prog. Phys. **62**, 859 (1999).
- C. M. Fowler, W. B. Garn, and R. S. Caird, J. Appl. Phys. **31**, 588 (1960).
- A. D. Sakharov, Sov. Phys. Usp. **9**, 294 (1966).
- F. S. Felber, M. A. Liberman, and A. L. Velikovich, Phys. Fluids **31**, 3675 (1988); F. S. Felber *et al.*, J. Appl. Phys. **64**, 3831 (1988).
- R. C. Kirkpatrick, I. R. Lindemuth, and M. S. Ward, Fusion Technol. **27**, 201 (1995).

11. O. V. Gotchev, N. W. Jang, J. P. Knauer, M. D. Barbero, R. Betti, C. K. Li, and R. D. Petrasso, *J. Fusion Energy* **27**, 25 (2008).
12. M. A. Liberman and A. L. Velikovich, *J. Plasma Phys.* **31**, 381 (1984).
13. A. Hasegawa *et al.*, *Phys. Rev. Lett.* **56**, 139 (1986).
14. T. R. Boehly, D. L. Brown, R. S. Craxton, R. L. Keck, J. P. Knauer, J. H. Kelly, T. J. Kessler, S. A. Kumpan, S. J. Loucks, S. A. Letzring, F. J. Marshall, R. L. McCrory, S. F. B. Morse, W. Seka, J. M. Soures, and C. P. Verdon, *Opt. Commun.* **133**, 495 (1997).
15. J. P. Knauer, O. V. Gotchev, P. Chang, D. D. Meyerhofer, R. Betti, F. H. Séguin, C. K. Li, J. A. Frenje, and R. D. Petrasso, presented at the Innovative Confinement Concepts Workshop and US-Japan Workshop on Improvement in the Confinement of Compact Torus Plasmas, Reno, NV, 24–27 June 2008.
16. O. V. Gotchev, J. P. Knauer, P. Y. Chang, N. W. Jang, M. J. Shoup III, D. D. Meyerhofer, and R. Betti, *Rev. Sci. Instrum.* **80**, 043504 (2009).
17. C. K. Li, F. H. Séguin, J. A. Frenje, J. R. Rygg, R. D. Petrasso, R. P. J. Town, P. A. Amendt, S. P. Hatchett, O. L. Landen, A. J. Mackinnon, P. K. Patel, V. Smalyuk, J. P. Knauer, T. C. Sangster, and C. Stoeckl, *Rev. Sci. Instrum.* **77**, 10E725 (2006).
18. J. R. Rygg, F. H. Séguin, C. K. Li, J. A. Frenje, M. J.-E. Manuel, R. D. Petrasso, R. Betti, J. A. Delettrez, O. V. Gotchev, J. P. Knauer, D. D. Meyerhofer, F. J. Marshall, C. Stoeckl, and W. Theobald, *Science* **319**, 1223 (2008).
19. C. K. Li, F. H. Séguin, J. R. Rygg, J. A. Frenje, M. Manuel, R. D. Petrasso, R. Betti, J. Delettrez, J. P. Knauer, F. Marshall, D. D. Meyerhofer, D. Shvarts, V. A. Smalyuk, C. Stoeckl, O. L. Landen, R. P. J. Town, C. A. Back, and J. D. Kilkenny, *Phys. Rev. Lett.* **100**, 225001 (2008).
20. F. H. Séguin, J. A. Frenje, C. K. Li, D. G. Hicks, S. Kurebayashi, J. R. Rygg, B.-E. Schwartz, R. D. Petrasso, S. Roberts, J. M. Soures, D. D. Meyerhofer, T. C. Sangster, J. P. Knauer, C. Sorce, V. Yu. Glebov, C. Stoeckl, T. W. Phillips, R. J. Leeper, K. Fletcher, and S. Padalino, *Rev. Sci. Instrum.* **74**, 975 (2003).
21. S. Agostinelli *et al.*, *Nucl. Instrum. Methods Phys. Res. A* **506**, 250 (2003).
22. N. W. Jang, R. Betti, J. P. Knauer, O. Gotchev, and D. D. Meyerhofer, *Bull. Am. Phys. Soc.* **51**, 144 (2006).